Bonding insights from structural and spectroscopic comparisons of {SnW_5} and {TiW_5} alkoxido- and aryloxido-substituted Lindqvist polyoxometalates.

Balamurugan Kandasamy,[a, b] Peter G. Bruce,[b,c] William Clegg,[a] Ross W. Harrington,[a] Antonio Rodríguez-Fortea,[d] Magda Pascual-Borrás[d] and R. John Errington*[a]

Dedicated to Prof. W. G. Klemperer on the occasion of his 70th birthday.

Abstract: Incorporation of $\{MX\}^{n+}$ groups into polyoxometalates (POMs) provides the means not only to introduce reactivity and functionality but also to tune the electronic properties of the oxide framework by varying M, X and *n*. In order to elucidate the factors responsible for differences in reactivity between {TiW_5} and {SnW_5} Lindqvist-type hexametalates, a series of alkoxido- and aryloxido-tin substituted POMs (nBu$_4$N)$_3$[(RO)SnW_5O_{18}] (R = Me, Et, *i*Pr and *t*Bu) and (nBu$_4$N)$_3$[(ArO)SnW_5O_{18}] (Ar = C_6H_5, 4-MeC_6H_5, 4-*t*BuC_6H_5, 4-HOC_6H_4, 3-HOC_6H_4 and 2-$CHOC_6H_4$) has been structurally characterised and studied by multinuclear NMR (^{1}H, ^{13}C, ^{17}O, ^{119}Sn and ^{183}W) and FTIR spectroscopy. Spectroscopic and structural parameters were compared with those of titanium-substituted homologues and, when coupled with theoretical studies, indicated that Sn–OR and Sn–OAr bonds are ionic with little π-contribution, whereas Ti–OR and Ti–OAr bonds are more covalent with π-bonding that is more prevalent for Ti–OR than Ti–OAr. This experimental and theoretical analysis of bonding in a homologous series of reactive POMs is the most extensive and detailed to date, and reveals factors which account for significant differences in reactivity between tin and titanium congeners.

Introduction

Polyoxometalates (POMs) of the Groups 5 and 6 transition metals V, Nb, Ta, Mo and W generally involves the aggregation (self-assembly) of small molecular precursors through protonation-condensation reactions in aqueous or non-aqueous media, but the rational design and synthesis of POMs with pre-determined structure and composition remains a major challenge that must be addressed if POMs are to be engineered for specific applications. POM self-assembly is still poorly understood, but progress is being made with regard to systematic post-functionalisation, *i.e.* the controlled modification of derivatised POM core units.[1] The rational, designed incorporation of reactive sites and/or organic functionality is therefore an important aspect of current POM research and enables fine-tuning of POM reactivity and covalent, rather than electrostatic, incorporation of POM units into functional materials. By exploiting the sensitivity of metal alkoxides towards hydrolysis, we have developed non-aqueous routes to a range of tetrabutylammonium (TBA) salts of heterometallic, Lindqvist-type {M′M_5} hexametalates [(RO)M′W_5O_{18}]$^{n-}$ (M′ = Ti, Zr, Hf, Nb, Sn) and [(RO)$TiMo_5O_{18}$]$^{n-}$.[2, 3] Modifications to the methodology also provided access to Co(II) derivatives [($CoW_5O_{18}H)_2$]$^{6-}$ and [(C_5H_5N)$CoW_5O_{18}H$]$^{3-}$.[4] The alkoxido-substituted hexametalates provide a platform for detailed solution reactivity studies as well as systematic access to a wide range of [XM′M_5O_{18}]$^{3-}$ derivatives (M = W, M′ = Ti, Zr; M = Mo, M′ = Ti).[5] Incorporation of these reactive sites also allowed us to achieve the first covalent attachment of a POM to silicon surfaces.[6] At a fundamental level, the incorporation of heterometal sites into the Lindqvist structure is expected to introduce electronic perturbations that may be investigated both spectrosopically and structurally. For example, the ^{183}W NMR spectra of [(MeO)TiW_5O_{18}]$^{3-}$ and [(MeO)SnW_5O_{18}]$^{3-}$ were found to be markedly different, showing that the properties of these isostructural POMs are not determined simply by the anion charge.[2(b)] Given that our synthetic approach facilitates the systematic manipulation of the ligand appended to the heterometal in [XM′M_5O_{18}]$^{3-}$ anions, we were therefore interested in expanding the range of [XSnW_5O_{18}]$^{3-}$ Lindqvist-type POMs for more detailed comparisons with their titanium-substituted congeners in order to understand specific bonding differences at the heterometal site. We report here the synthesis and characterisation of a range of alkoxido and aryloxido derivatives [(RO)SnW_5O_{18}]$^{3-}$, derived from [(MeO)SnW_5O_{18}]$^{3-}$ **1** by protonolysis of the Sn–OMe bond. Detailed spectroscopic and structural comparisons with titanium-substituted analogues, coupled with theoretical computational studies, have identified important factors associated with bonding variations in these {MW_5} heterometallic POMs that are key to understanding differences in reactivity. The main feature of this work is that the $\{MOR\}^{3+}$ fragments are embedded within a totally inorganic environment, which is more likely to reflect the electronic properties of solid oxides than organometallic or metalorganic complexes that have been investigated as models for surface oxide reactivity.

[a] Dr. B. Kandasamy, Prof. W. Clegg, Dr R. W. Harrington, Dr. R. J. Errington
School of Chemistry, Newcastle University, Newcastle upon Tyne, NE1 7RU, UK
E-mail: John.Errington@newcastle.ac.uk
[b] Prof. P. Bruce, Dr. B. Kandasamy (previous address)
School of Chemistry, University of St. Andrews, St. Andrews, KY16 9ST, UK
[c] Prof. P. Bruce,
Department of Materials, University of Oxford, Parks Road, Oxford, OX1 3PH, UK
[d] Dr. A. Rodriguez-Fortea, Dr. M. Pascual-Borrás.
Departament de Química Física i Inorgànica, Universitat Rovira i Virgili, C/ Marcel·lí Domingo 1, 43007 Tarragona, Spain

Supporting information for this article is given via a link at the end of the document.

Results and Discussion

Metathesis of the methoxido ligand in $(TBA)_3$**1** was achieved as shown in Equation 1 by treatment with an excess of the alcohol or phenol at elevated temperatures (85 - 90 °C) in acetonitrile, to give high yields of TBA salts of anions **2** - **10**. Although protonolysis of $(TBA)_3$**1** proceeded more rapidly than that of $(TBA)_3[(MeO)TiW_5O_{18}]$, an excess of HX reagent and prolonged heating was used to ensure high conversions. It is also worth noting that the alkoxido species $[(RO)SnW_5O_{18}]^{3-}$ are much more moisture-sensitive than their titanium analogues and the slightest traces of water produced small amounts of $[(HO)SnW_5O_{18}]^{3-}$ in solution. Reactions were monitored conveniently by ^{119}Sn NMR spectroscopy and by ^{17}O NMR spectroscopy when ^{17}O-enriched $(TBA)_3$**1** was used as the starting material. Products were also characterised by ^{1}H, ^{13}C and ^{183}W NMR spectroscopy and by single-crystal X-ray diffraction. ^{119}Sn, ^{183}W and ^{17}O NMR data for the $(TBA)_3[XSnW_5O_{18}]$ products are given in Table S1, crystallographic data in Table S2 and selected bond lengths and angles for non-structurally disordered compounds in Table S3.

$$[(MeO)SnW_5O_{18}]^{3-} + HX \rightleftharpoons [XSnW_5O_{18}]^{3-} + MeOH \qquad (1)$$

1

	X		
2	OEt	**5**	OPh
3	O*i*Pr	**6**	OC_6H_4Me-4
4	O*t*Bu	**7**	$OC_6H_4{}^tBu$-4
		8	OC_6H_4OH-3
		9	OC_6H_4OH-4
		10	OC_6H_4CHO-2

It is generally accepted that alcoholysis of primary alkoxido ligands becomes less favourable with increasing ramification of the incoming secondary or tertiary alkoxido groups.[7] However, it was possible to replace the OMe group in $(TBA)_3$**1**, not only by OEt but also by O*i*Pr and O*t*Bu by using a large excess of the respective alcohol, which also served to suppress trace hydrolysis. Similarly, reactions with an excess of the more acidic phenols proceeded to completion at elevated temperatures. Substitution was confirmed by the absence of the SnOMe peak at 3.64 ppm in the ^{1}H NMR spectra of the products, the presence of peaks for the alkoxido or aryloxido groups in addition to TBA counter-cation peaks in ^{1}H and ^{13}C NMR spectra, and by new resonances in ^{119}Sn NMR spectra. In addition, ^{17}O and ^{183}W NMR spectra were consistent with mono-substituted, C_{4v} symmetrical $[XSnW_5O_{18}]^{3-}$ anions.

Hence, ^{17}O NMR spectra contained two peaks for the four equivalent equatorial and the single axial terminal W=O groups, one peak for bridging SnOW, two peaks for bridging WOW and one for the central μ_6-O atom, while two peaks in ^{183}W NMR spectra could be assigned to the four equivalent equatorial tungsten atoms and the unique axial tungsten atom (Table 1). IR spectra for alkoxides $(TBA)_3$**2**, $(TBA)_3$**3** and $(TBA)_3$**4** in Figure S1 show ν(W=O) at 952-953 cm^{-1} and strong bands at 800-803 and 755-758 cm^{-1} for vibrations associated with SnOW and WOW bridges. Corresponding bands in the IR spectra of TBA salts of aryloxides **5** - **10** occur in the regions 953-958, 799-804 and 748-755 cm^{-1} respectively (Figure S2). In addition, broad bands for ν(OH) were observed at 3294 and 3260 cm^{-1} in the IR spectra of $(TBA)_3$**8** and $(TBA)_3$**9** respectively while ν(CO) for the aldehyde group in $(TBA)_3$**10** appeared at 1679 cm^{-1}.

Single crystals for X-ray crystallographic studies were grown from MeCN solutions and crystallographic data are collected in Table S2. As was the case for $(TBA)_3$**1**,[2b] disorder was problematic in the crystal structure of $(TBA)_3$**2**, in which the least disordered anion shows two-fold disorder of the {SnOEt} group across opposite positions in the hexametalate, while on the other crystallographic site two $[(EtO)SnW_5O_{18}]^{3-}$ anions are superimposed, with {SnOEt} groups in opposite positions and SnOW axes rotated by 11 – 12 ° relative to each other (Figure S3). Such anion disorder was not present in the crystal structures of $(TBA)_3$**3** and $(TBA)_3$**4**, which contained four and two independent anions respectively, selected structures of which are shown in Figure 1 (a) and (b) respectively. The anions in the crystal structures of the aryloxido compounds $(TBA)_3$**5**, $(TBA)_3$**6**, $(TBA)_3$**7** and $(TBA)_3$**10** were not disordered and the structures shown in Figure 1 (c) – (f) feature aryl planes that lie between Sn–OW bonds, bisecting the two vertical planes containing Sn and W_{ax} with OSnOC torsion angles of 34° (**5**), 45° (**6**), 46° (**7**) and 45° (**10**), similar to those in analogous {TiW_5} anions.[5a] In **10** the aldehyde group does not interact with Sn, adopting a distal position as in the Ti analogue,[5a] and in contrast to the chelating bonding mode observed in the zirconium analogue that contains seven-coordinate zirconium.[5b] The {$SnOC_6H_4OH$-4} or {$SnOC_6H_4OH$-3} groups in the structures of the 4- and 3-hydroxy-substituted phenoxides $(TBA)_3$**8** and $(TBA)_3$**9** displayed two-fold disorder over opposite positions, with H-bonding to *trans*-disordered terminal W=O from adjacent anions to give disordered chains as shown in Figure S4. For comparison purposes, selected bond distances and angles for only the non-disordered {SnW_5} structures are collected in Table S3.

Spectroscopic and structural comparisons

To assess the electronic effects of ligand (X) and heterometal (M) variation in $[XMW_5O_{18}]^{3-}$ anions (M = Ti, Sn), we have been able to compare for the first time the extensive spectroscopic and structural data for this series of {SnW_5} hexametalates with those for their {TiW_5} homologues. The reactivity of these heterometallic POMs will be determined largely by the nature of the M–X bonds and, in alkoxido and aryloxido species, Sn–O bonds are expected to be more ionic than Ti–O bonds,[10] with a greater likelihood of oxygen to metal π–bonding in the titanium-substituted anions because of the availability of empty 3d orbitals. Charge distribution within these POMs and the electronic environments of the constituent atoms may be investigated by multinuclear NMR spectroscopy (^{119}Sn, ^{183}W and ^{17}O), and in FTIR spectra ν(W=O) and ν(WOW) vibrations are sensitive to the charge density on the metal oxide framework. Averaged NMR and FTIR spectroscopic parameters for equivalent alkoxido (OR) and aryloxido (OAr) derivatives of {SnW_5} and {TiW_5} hexametalates are given in Table 1, with averaged M–OC bond lengths and MOC angles in Table 2.

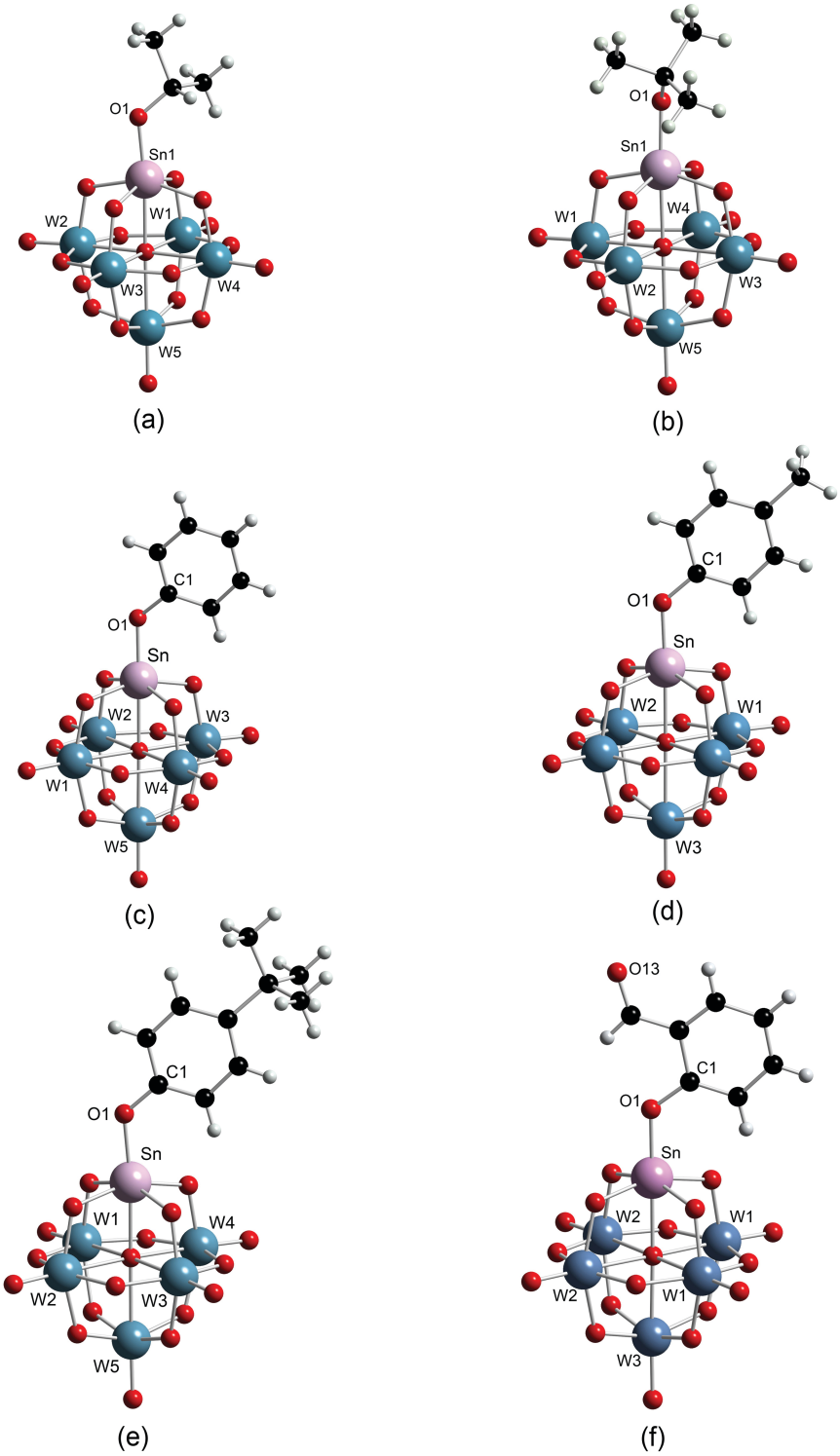

Figure 1. Structures of (a) one of the four independent $[(i\text{PrO})SnW_5O_{18}]^{3-}$ anions in the crystal structure of $(TBA)_3$**3**, (b) one of the two independent $[(t\text{BuO})SnW_5O_{18}]^{3-}$ anions in the crystal structure of $(TBA)_3$**4**, (c) the anion $[(PhO)SnW_5O_{18}]^{3-}$ **5**, (d) the anion $[(4\text{-}MeC_6H_4O)SnW_5O_{18}]^{3-}$ **6**, (e) the anion $[(4\text{-}t\text{BuC}_6H_4O)SnW_5O_{18}]^{3-}$ **7** and (f) the anion $[(2\text{-}CHOC_6H_4O)SnW_5O_{18}]^{3-}$ **10**.

Table 1. Average spectroscopic parameters for {XMW_5} polyoxometalates (M = Ti, Sn)

Anion[a]	^{119}Sn chemical shift/ppm [$^2J\{^{119}Sn^{183}W_{eq}\}$/Hz]	^{183}W chemical shift/ppm		^{17}O chemical shift/ppm				ν(W–O)/cm^{-1}	
		W_{eq}	W_{ax}	W=O	MOW	WOW	μ_6-O	W=O	WOW
$[(RO)SnW_5O_{18}]^{3-}$	–654(6) [40(1)]	75(2)	–128(1)	724(2), 684(1)	396(1)	383(1), 366(2)	18(1)	953(1)	757(1)[b]
$[(ArO)SnW_5O_{18}]^{3-}$	–673(1) [47(2)]	78(1)	–123(1)	723(1), 689(1)	397(1)	386(1), 362(1)	16(1)	956(2)	752(2)[b]
$[(RO)TiW_5O_{18}]^{3-}$		40(5)	74(6)	722(1), 714(1)	527(1)	392(1), 381(1)	–57(1)	946(1)	775(1)
$[(ArO)TiW_5O_{18}]^{3-}$		22(3)	66(3)	727(1), 717(1)	534(2)	394(1), 384(1)	–49(3)	952(2)	789(5)

[a] As nBu$_4$N$^+$ salts. [b] an additional band at ca. 800 cm^{-1} for {SnW_5} anions was tentatively assigned to ν(Sn–O).

{SnW$_5$} anions

Within the series of {SnW_5} anions, the minimal differences in Sn–OC bond lengths and SnOC angles between SnOR and SnOAr substituted anions indicate that the nature of the Sn–OC bonding is similar in alkoxido and aryloxido derivatives, although ^{119}Sn chemical shifts for SnOR alkoxido anions are downfield of those for SnOAr and $^2J(^{119}Sn^{183}W)$ coupling constants are smaller for SnOR derivatives, which may indicate a subtle difference in charge distribution that is not reflected in the structural parameters. In ^{183}W NMR spectra, the average values for $\delta(W_{eq})$ and $\delta(W_{ax})$ for {$(RO)SnW_5$} derivatives are similar to those for {$(ArO)SnW_5$} derivatives, as are the average ^{17}O NMR and FTIR spectral parameters, again suggesting little variation in Sn–OC bonding between the two types of anions.

{TiW$_5$} anions

Within the series of {TiW_5} anions, the average Ti–OC bond length is generally shorter for TiOR derivatives which, together with an average TiOC angle of 157(4) ° for the alkoxides, is consistent with the presence of some O to Ti π-bonding in the {$(RO)TiW_5$} species. The greater variation in TiOC angle for the {$(ArO)TiW_5$} species gives a larger estimated error in the average value, which means that this is a less reliable indicator of π-bonding in the {$(ArO)TiW_5$} species and the angle is likely to be affected more by steric pressure than bonding constraints, as discussed previously by Rothwell.[8] There are differences in ^{183}W NMR spectra; $\delta(W_{eq})$ and $\delta(W_{ax})$ for {$(RO)TiW_5$} anions are downfield of those for {$(ArO)TiW_5$} anions and the magnitude of the average chemical shift difference $|\delta(W_{eq}) - \delta(W_{ax})|$ is smaller (34 ppm) for the more strongly π-bonded alkoxides than for the aryloxides (44 ppm). In the ^{17}O NMR spectra, the TiOW and central μ_6-O peaks of {$(RO)TiW_5$} anions are slightly upfield of those for {$(ArO)TiW_5$} anions. The average ν(W=O) and ν(WOW) absorptions in FTIR spectra of {$(RO)TiW_5$} anions occur at lower wavenumbers than the corresponding vibrations for {$(ArO)TiW_5$} anions, indicating that O to Ti π-bonding slightly increases the electron density on the oxometalate core.

Effects of Sn vs Ti substitution

It has been proposed that the nature of M–O bonds in metal alkoxides ranges from about 65% ionic for elements with electronegativities on the Pauling scale of 1.5 – 1.3 to about 80 % ionic for more electropositive elements with electronegativities 1.2 – 0.9.[7] Therefore, based on electronegativity, Ti–OR bonds would be expected to be more polar than Sn–OR bonds, as the Pauling electronegativity values for Ti and Sn are 1.54 and 1.96 respectively. However, in the case of Ti, the availability of 3d orbitals enables oxygen to Ti π-bonding, which will increase the covalency of the Ti–O bonds. When comparing {SnW_5} and {TiW_5} alkoxido and aryloxido homologues, it is evident that Sn–OC bonds are longer than the Ti–OC bonds, while the SnOC angles are smaller than the TiOC angles (Table 2). This is consistent with the more ionic nature of Sn–OC bonding and the absence of O to Sn π-bonding and is represented graphically in Figure 2.

Table 2. Average M–OC bond distances (Å) and MOC angles (°) for {XMW_5} polyoxometalates (M = Ti, Sn)

Anion[a]	M–O	MOC
$[(RO)SnW_5O_{18}]^{3-}$	1.959(19)	128(7)
$[(ArO)SnW_5O_{18}]^{3-}$	1.973(16)	128(2)
$[(RO)TiW_5O_{18}]^{3-}$	1.770(15)	157(4)
$[(ArO)TiW_5O_{18}]^{3-}$	1.83(4)	148(14)

[a] As nBu$_4$N$^+$ salts.

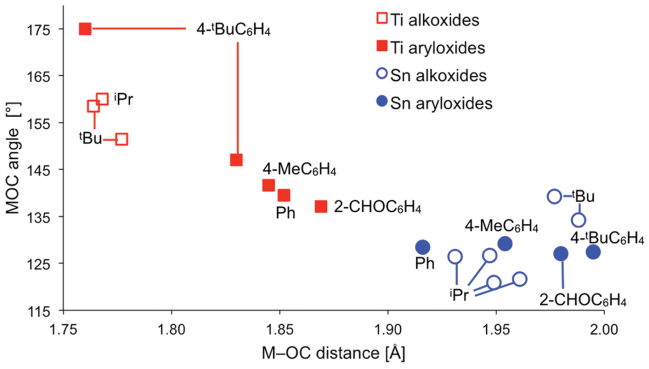

Figure 2. Plot of M–OC bond length *vs.* MOC bond angle from non-disordered anions in crystal structures of $(TBA)_3[(RO)MW_5O_{18}]$ and $(TBA)_3[(ArO)MW_5O_{18}]$.

Note that data for the two anions in the crystal structure of $(TBA)_3[(4\text{-}t\text{BuC}_6H_4O)TiW_5O_{18}]$ are much less precise than for the other anions, otherwise trends for $\{TiW_5\}$ anions are generally consistent with expected effects of aryl substituents.

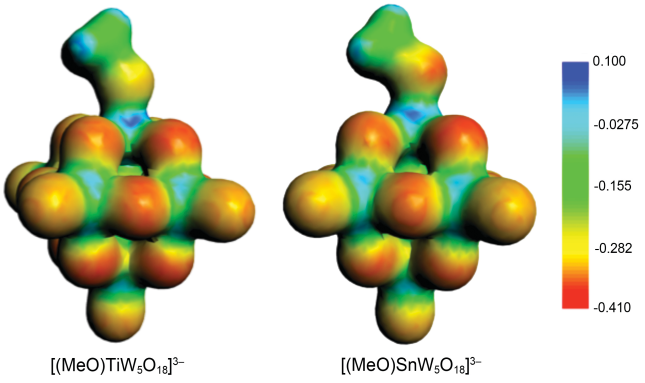

Figure 3. Calculated molecular electrostatic potentials for $[(MeO)MW_5O_{18}]^{3-}$ anions (M = Ti, Sn). The more negative regions are coloured red and the more positive regions blue.

Table 3. Atomic charges (Bader partition) for M (Sn and Ti), and the MOC and MOW oxygen atoms bonded to M in $[(MeO)MW_5O_{18}]^{3-}$ anions.

Atom	M = Sn	M = Ti
M	2.367	2.176
MOW(1)	–1.090	–1.053)
MOW(2)	–1.090	–1.053
MOW(3)	–1.097	–1.066
MOW(4)	–1.097	–1.066
MOC	–1.057	–1.022

Calculated molecular electrostatic potentials and atomic charges for $[(MeO)MW_5O_{18}]^{3-}$ anions (M = Ti, Sn) are compared in Figure 3 and Table 3 respectively, and are consistent with the bonding differences discussed above, such that oxygen atoms bonded to M are more negatively charged when M = Sn, and Sn is more positively charged than Ti. Another key feature is that the MOW oxygens are more negative than the alkoxido MOC oxygens. Importantly, these factors will determine the reactivity of these anions such that Sn is expected to be more electrophilic than Ti and the protons of protic reagents such as alcohols or water might interact initially with MOW rather than MOC. This will be discussed in more detail in a forthcoming paper describing the comparative reactivity of $\{(RO)MW_5\}$ Lindqvist and $\{(MeO)MPW_{11}\}$ Keggin type POMs towards protonolysis.

Differences in charge distribution within the $[(RO)MW_5O_{18}]^{3-}$ anions are reflected in the average NMR parameters shown in Table 1. The most noticeable features of the $\{SnW_5\}$ ^{17}O NMR spectra were the significant upfield shift of SnOW peaks and the downfield shift of the central μ_6-O peak compared to the corresponding peaks for $\{TiW_5\}$ anions. While the upfield shift of SnOW compared to TiOW is reminiscent of upfield shifts observed upon addition of electrophiles to TiOW bridging oxygens,[9] this clearly does not reflect a lower basicity for SnOW, as shown by the calculated electrostatic potentials and atomic charges, but rather may arise from a smaller electronegativity difference between Sn and W than between Ti and W. It is also evident that ^{17}O NMR peaks for terminal W_{ax}=O *trans* to Sn appear upfield of those for W_{ax}=O *trans* to Ti, while those for W_{eq}=O situated *cis* to Ti or Sn have similar chemical shifts. This apparent electronic *trans*-influence is even more striking in ^{183}W NMR spectra, where resonances for W_{ax} *trans* to Sn in $\{SnW_5\}$ anions are shifted significantly upfield compared to those for W_{ax} *trans* to Ti in $\{TiW_5\}$ anions, such that $|\delta(W_{eq}) - \delta(W_{ax})|$ values of *ca.* 200 ppm are much larger for $\{SnW_5\}$ anions. This significant feature was probed further by DFT calculations, which are discussed in more detail below.

DFT calculations of ^{183}W NMR chemical shifts

Modern computational methods are able to predict the spectroscopic properties of POMs with increasing accuracy.[10] Given the remarkable difference in magnitude of $\delta(W_{eq}) - \delta(W_{ax})$ between analogous $\{XSnW_5\}$ and $\{XTiW_5\}$ anions, we were interested to see whether a computational analysis of $[(MeO)SnW_5O_{18}]^{3-}$ and $[(MeO)TiW_5O_{18}]^{3-}$ would predict relative ^{183}W NMR chemical shifts and $^2J(^{119}Sn^{183}W)$ spin-spin coupling constants that were similar to experimentally observed values. Calculations were performed for two conformations with C_s symmetry and OSnOC torsion angles of either 0 ° (eclipsed) or 45 ° (staggered) to simulate rotation of the CH_3 group around the Sn–O bond, and results are summarized in Tables S4 and S5. Although the absolute errors in the prediction of the shifts are not negligible, −91 *vs* −128 ppm for W_{ax} and 104 *vs* 77 ppm for the W_{eq}, the experimental trend is well reproduced and, moreover, the separation between the two predicted peaks (195 ppm) is close to the experimental value (205 ppm), showing that the predicted chemical shifts for the two different types of W atoms (W_{ax} and W_{eq}) are both shifted around 30 ppm from the experimental value. This suggests that the same type of error is present in the prediction of the shielding of the two types of W atoms or in the prediction of the shielding of the reference. The average magnitudes of $^2J(^{119}Sn^{183}W)$ calculated for the two conformers also provide very good estimates of the experimental values, *i.e.* 9.3 *vs* 12 Hz for $^2J(^{119}Sn^{183}W_{ax})$ and 39.7 *vs* 38 Hz, for $^2J(^{119}Sn^{183}W_{eq})$. It was not possible to determine the signs of $^2J(^{119}Sn^{183}W)$ from our experiments. Table 4 compares results for the staggered conformations of $[(MeO)SnW_5O_{18}]^{3-}$ and $[(MeO)TiW_5O_{18}]^{3-}$. For the Ti derivative the absolute errors in the prediction of the shifts are higher than for the Sn derivative, +145 *vs* +65 ppm for W_{ax} and 102 *vs* 32 ppm for the W_{eq}, but the relative chemical shifts for W_{eq} and W_{ax} are well reproduced. Notably, the experimental $(\delta(W_{eq}) - \delta(W_{ax}))$ values of +205 ppm for the $\{SnW_5\}$ anion and −33 ppm for the $\{TiW_5\}$ anion compare well with the computed values of +195 and −43 ppm, respectively. Therefore, while the absolute ^{183}W chemical shifts are not well reproduced for these anions, the trends are very well predicted. The different behaviour for $\{TiW_5\}$ and $\{SnW_5\}$ anions seems to have an electronic origin because when we used the optimized geometry for $[(MeO)SnW_5O_{18}]^{3-}$ and replaced Sn by Ti without relaxing the geometry, the shift computed for $\delta(W_{ax})$ is + 65 ppm, whereas the value calculated for $[(MeO)SnW_5O_{18}]^{3-}$ was –91 ppm. Attempts to analyse the molecular orbital contributions to the paramagnetic shielding, σ_p, (Figure S5) did not show any dominant terms that might provide a simple chemical explanation for the dramatically different values observed for $\delta(W_{ax})$.

Table 4. Calculated and experimental NMR parameters for anions $[(MeO)TiW_5O_{18}]^{3-}$ and $[(MeO)SnW_5O_{18}]^{3-}$ [a]

	$[(MeO)SnW_5O_{18}]^{3-}$		$[(MeO)TiW_5O_{18}]^{3-}$	
	Calc	Exp	Calc	Exp
$\delta(W_{eq})$/ppm	104.1	76.9	102	32
$\delta(W_{ax})$/ppm	–90.5	–128.1	145	65
$\delta(W_{eq}) - \delta(W_{ax})$/ppm	195	205	–43	–33
$^2J(^{119}Sn^{183}W_{eq})$/Hz	–39.7	38	-	-
$^2J(^{119}Sn^{183}W_{ax})$/Hz	–9.3	12	-	-

[a] DFT calculations at BP86 level using a TZP basis set for the chemical shifts and a TZ2P basis set for spin-spin couplings (see Computational Details).

Conclusions

Synthesis methods developed in our laboratory have enabled extensive structural and spectroscopic studies of a homologous series of alkoxido and aryloxido {SnW_5} and {TiW_5} Lindqvist type POMs. Differences between homologues can be rationalised in terms of the nature of the M–OR and M–OAr bonds with regard to the degree of ionicity and π-bonding. Structurally, the M–OR and M–OAr bond lengths and MOC angles are consistent with a greater degree of ionicity for Sn–OC bonds, while π-bonding is apparent for Ti–OC bonds. The spectroscopic properties of these POMs reflect different charge distributions in {TiW_5} and {SnW_5} homologues that are consistent with theoretical calculations of molecular electrostatic potentials and atomic charges. Electronic effects appear to be transmitted across the Lindqvist anions to the axial W=O group *via* a *trans* influence and the dramatic differences in ^{183}W NMR spectra of {TiW_5} and {SnW_5} anions has been modeled by DFT, although no simple link between the differences in paramagnetic shielding and molecular orbital contributions has been identified. This is the most detailed and extensive study of a homologous series of derivatised POMs to date and the insights provided have important implications for the reactivity of {XMW_5} Linqvist anions, *e.g.* the greater hydrolytic sensitivity of M–OR bonds in $[(RO)SnW_5O_{18}]^{3-}$ anions compared to {TiW_5} homologues, and may also provide insight into oxide surface reactivity. The greater charge density associated with MOW compared to MOR is also likely to influence the interaction of these anions with protic reagents. The mechanistic consequences of these bonding differences have been explored in detailed experimental and theoretical studies of hydrolytic and protonation behaviours of alkoxido-substituted Lindqvist type $[(MeO)MW_5O_{18}]^{3-}$ and Keggin-type $[(MeO)MPW_{11}O_{39}]^{4-}$ anions (M = Ti, Sn), the results of which will be published separately.

Experimental Section

All reactions and manipulations were carried out under an atmosphere of dry, oxygen-free nitrogen in screw-top flasks fitted with J Young PTFE screw valves using Schlenk and dry-box techniques.[11] Hydrocarbon and ether solvents were dried over and distilled from sodium benzophenone ketyl, acetonitrile was dried over and distilled from calcium hydride and alcohols ROH (R= Me, Et) were pre-dried over 3A molecular sieves and distilled from the corresponding magnesium alkoxide. All solvents were stored over 3A molecular sieves under dry nitrogen. Phenol, p-Cresol and salicylaldehyde (Sigma Aldrich) were sublimed or distilled and stored under nitrogen. 4-tert-butylphenol, hydroquinone and resorcinol were purchased from Sigma Aldrich and used without further purification. ^{17}O-enriched and non-enriched $(TBA)_3[(MeO)SnW_5O_{18}]$ was synthesised according to a published procedure[2(b)] and the purity was confirmed by ^{1}H, ^{17}O and ^{119}Sn NMR and FTIR spectroscopy. 10% ^{17}O-enriched water and deuteriated acetonitrile were purchased from Goss Scientific. The latter was degassed and stored under nitrogen over calcium hydride or 3A molecular sieves.

Infrared spectra were recorded on a Varian 800 FTIR spectrometer from Nujol mulls between CsI or KBr plates. NMR spectra were recorded on a Bruker Avance 300 spectrometer operating at 300.0 MHz (^{1}H) or 75.39 MHz (^{13}C), a Jeol ECS 400 spectrometer operating at 100.5 MHz (^{13}C) or 149.08 MHz (^{119}Sn), or a Jeol Lamda 500 spectrometer operating at 500.0 MHz (^{1}H), 125.65 MHz (^{13}C), 67.81 MHz (^{17}O), 186.5 MHz (^{119}Sn) and 20.84 MHz (^{183}W). NMR spectra were referenced by sample replacement to $SiMe_4$ (^{1}H and ^{13}C), water (^{17}O), $SnMe_4$ (^{119}Sn) and aqueous 2M Na_2WO_4 (^{183}W). Coupling constants are given in Hz. Resonances due to nBu$_4$N$^+$ cations are not listed in the ^{1}H and ^{13}C NMR data given below, but appear as multiplets centred at about 1.0, 1.4, 1.7 and 3.2 ppm in ^{1}H NMR spectra and as singlets at about 13, 19, 24 and 58 ppm in ^{13}C{^{1}H} NMR spectra. C, H and N analyses were performed by the Newcastle University chemical analysis unit.

All single-crystal diffraction data were collected at 150 K on an Oxford Diffraction Gemini A Ultra diffractometer with Mo$K\alpha$ radiation (λ = 0.71073 Å). Absorption corrections were applied using a semi-empirical multiscan method along with interframe scaling.[12] The structures were solved by automatic direct methods and refined by full-matrix least-squares on all unique F^2 values,[13] with hydrogen atoms constrained in a riding model. Extensive disorder in some of the cations (**4**, **5**, **6**, **8**, **9**, **10**) was modelled as far as possible with the aid of restraints on geometry and anisotropic displacement parameters, though unresolved disorder clearly remains in some cases; anions of **2**, **8** and **9** have disorder of Sn and W atom positions as a consequence of crystallographic symmetry. The structures of **5** and **7**, in non-centrosymmetric space groups, display partial inversion twinning.

DFT calculations were performed with the ADF2016 package.[14] We applied the local density approximation featuring the Xα model with Becke's functional for exchange and the VWN parameterization with Perdew's correction for correlation. The NMR calculations were performed with a Slater-TZP-quality basis set (TZ2P for the spin-spin coupling constants) to describe the valence-shell electrons. We applied spin-orbit relativistic corrections to them within the zeroth-order regular approximation (ZORA). The solvent effects were taken into account *via* the COSMO (Conductor-like Screening Model) procedure (acetonitrile, ε = 37.5). The quality of the geometry is extremely relevant in the study of NMR chemical shifts as shown previously,[10f] so the geometries were computed using a very large basis set of QZ4P quality.

$(TBA)_3[(EtO)SnW_5O_{18}]$, **$(TBA)_3$ 2** – Dry ethanol (2.2 mL, 37.3 mmol) was added to $(TBA)_3$**1** (0.78 g, 0.37 mmol) in dry acetonitrile (20 mL) and the mixture was heated at 90 °C for 12 h. After removal of volatile impurities under reduced pressure, the colourless residue was again treated with excess dry ethanol, and this process was repeated at least twice. The colourless crude product was washed with dry ether, (3 × 20 mL) and further recrystallised from acetonitrile by vapour diffusion of diethyl ether at room temperature to give colourless crystals. Yield 0.71 g, 90%. ^{1}H NMR (300 MHz, [D$_3$]MeCN, Me_4Si): δ = 1.19, (t, 3H, $^3J(^1H,^1H)$ = 6.9 Hz, $^4J(^1H,^{119}Sn)$ = 4.2 Hz, OCH_2CH_3) and 3.80 (q, 2H, $^3J(^1H,^1H)$ = 6.9 Hz, $^3J(^1H,^{119}Sn)$ = 69.6 Hz, $^3J(^1H,^{117}Sn)$ = 66.6 Hz, OCH_2CH_3); C{^{1}H} NMR

(100.53 MHz, [D$_3$]MeCN, Me$_4$Si): δ = 19.94, (^3J(^{13}C,$^{119,\ 117}$Sn) = 34.5 Hz, CH_2CH_3) and 60.6 (^2J(^{13}C,$^{119,\ 117}$Sn) = 35.45 Hz, CH_2CH_3); IR (Nujol): ν = 2729 m, 2409 m, 1655 m, 1378 s, 1309 w, 1152 m, 1097 m, 1058 m, 1027 m, 953 s, 885 m, 803 s, 758 s, 625 m, 569 m, 429 s cm^{-1}; elemental analysis calcd (%) for $C_{50}H_{113}N_3O_{19}SnW_5$: C 28.61, H 5.42, N 2.00; found: C 27.32, H 5.41, N 1.99.

(TBA)$_3$[(*i*PrO)SnW$_5$O$_{18}$], (**TBA)$_3$3** – Using the same procedure as for (TBA)$_3$**2** above, (TBA)$_3$**1** (0.77 g, 0.37 mmol) was treated with dry propan-2-ol (2.83 mL, 37 mmol). Yield 0.63 g, 79 %. ^{1}H NMR (300 MHz, [D$_3$]MeCN, Me$_4$Si): δ = 1.16, (d, 6H, ^3J(^{1}H,^{1}H) = 6.0 Hz, ^4J(^{1}H,^{119}Sn) = 3.3 Hz, CH(CH_3)$_2$) and 4.23 (septet, 1H, ^3J(^{1}H,^{1}H) = 6.0 Hz, ^3J(^{1}H,^{119}Sn) = 57.3 Hz, ^3J(^{1}H,^{117}Sn) = 54.9 Hz, CH(CH$_3$)$_2$); C{^{1}H} NMR (100.53 MHz, [D$_3$]MeCN, Me$_4$Si): δ = 26.7 (s, ^3J(^{13}C,^{119,117}Sn) = 34.5 Hz, HC(CH$_3$)$_2$) and 66.1 (s, ^2J(^{13}C,^{119,117}Sn) = 35.5 Hz, CH(CH$_3$)$_2$); IR (Nujol): ν = 2728 m, 1662 w, 1377 s, 1152 m, 1124 w, 1026 w, 953 s, 884 m, 803 s, 758 s, 623 m, 569 m, 430 s cm^{-1}; elemental analysis calcd (%) for $C_{51}H_{115}O_{19}N_3SnW_5$: C 28.99, H 5.48, N 1.98; found: C 27.87, H 5.21, N 2.00.

(TBA)$_3$[(*t*BuO)SnW$_5$O$_{18}$], **(TBA)$_3$4** – Using the same procedure as for (TBA)$_3$**2** above, (TBA)$_3$**1** (0.75 g, 0.36 mmol) was treated with dry *tert*-butyl alcohol (3.42 mL, 36 mmol). Yield 0.58 g, 75 %. ^{1}H NMR (300 MHz, [D$_3$]MeCN, Me$_4$Si): δ = 1.29, (s, 9H, ^4J(^{1}H,^{119}Sn) = 2.4 Hz, OC(CH_3)$_3$); C{^{1}H} NMR (100.53 MHz, [D$_3$]MeCN, Me$_4$Si): δ = 32.7 (s, ^3J(^{13}C,^{119,117}Sn) = 32.5 Hz, OC(CH_3)$_3$) and 71.5 (s, ^2J(^{13}C,^{119,117}Sn) not resolved, OC(CH$_3$)$_3$); IR (Nujol): ν = 2727 m, 1669 m, 1195 s, 1153 m, 1056 m, 1027 m, 952 s, 885 m, 800 s, 755 s, 624 m, 564 m, 425 s cm^{-1}; elemental analysis calcd (%) for $C_{52}H_{117}O_{19}N_3SnW_5$: C 29.37, H 5.55, N 1.97; found: C 30.2, H 5.92, N 2.00.

(TBA)$_3$[(C$_6$H$_5$O)SnW$_5$O$_{18}$], **(TBA)$_3$5** – Phenol (0.035 g, 0.366 mmol) was added to (TBA)$_3$**1** (0.69 g, 0.33 mmol) in acetonitrile (15 mL) and the mixture was heated at 90 °C for 24 h. After removal of volatiles under reduced pressure, the yellow residue was washed with dry THF (2 x 20 mL), dry toluene (2 x 20 mL) and dry diethyl ether (2 x 20 mL) to remove unreacted phenol. The pale yellow solid was recrystallised from acetonitrile by vapour diffusion of diethyl ether at room temperature to give pale yellow crystals. Yield 0.59 g, 82%. ^{1}H NMR (300 MHz, [D$_3$]MeCN, Me$_4$Si): δ = 6.79 (m, 1H, *p*-C$_6H_5$), 6.97 (m, 2H, *o*-C$_6H_5$) and 7.20 (m, 2H, *m*-C$_6H_5$); C{^{1}H} NMR (100.53 MHz, [D$_3$]MeCN, Me$_4$Si): δ = 118.8 (*p*-C$_6$H$_5$), 120.0 (^3J(^{13}C,^{119,117}Sn) = 31.6 Hz, *o*-C$_6$H$_5$), 129 (*m*-C$_6$H$_5$) and 161 (*ipso*-C$_6$H$_5$); IR (Nujol): ν = 2729 m, 2303 m, 1593 m, 1378 s, 1282 m, 1260 s, 1073 w, 1027 w, 957 s, 884 m, 804 s, 755 s, 621 m, 608 m 572 m, 432 s cm^{-1}; elemental analysis calcd (%) for $C_{54}H_{113}O_{19}N_3SnW_5$: C 30.22, H 5.30, N, 1.96; found: C 29.42, H 5.38, N 1.95.

(TBA)$_3$[(4-CH$_3$C$_6$H$_4$O)SnW$_5$O$_{18}$], **(TBA)$_3$6** – A solution of *p*-cresol (48.4 mg, 0.45 mmol) in acetonitrile (5 mL) was added to a solution of (TBA)$_3$**1** (0.85 g, 0.41 mmol) in acetonitrile (10 mL) and the mixture was heated at 90 °C for 30 h. After removal of volatiles under reduced pressure, the yellow residue was washed with dry THF (2 x 20 mL), dry toluene (2 x 20 mL) and dry diethyl ether (2 x 20 mL) to remove unreacted *p*-cresol. The pale yellow crude product was dried *in vacuo* and recrystallised from acetonitrile and diethyl ether at room temperature to give colourless crystals. Yield 0.72 g, 82 %. ^{1}H NMR (300 MHz, [D$_3$]MeCN, Me$_4$Si): δ = 2.24 (s, 3H, CH_3), 6.85 (m, 2H, C$_6H_4$) and 6.89 (m, 2H, C$_6H_4$); C{^{1}H} NMR (100.53 MHz, [D$_3$]MeCN, Me$_4$Si): δ = 19.7 (CH$_3$), 119.9 (^3J(^{13}C,^{119,117}Sn) = 30.7 Hz, *o*-C$_6$H$_4$), 127.7 (*p*-C$_6$H$_4$), 129.3 (*m*-C$_6$H$_4$) and 158 (^2J(^{13}C,^{119,117}Sn) = 36.7 Hz, *ipso*-C$_6$H$_4$); IR (Nujol): ν = 2729 m, 1608 m, 1508 s, 1378 s, 1272 m, 1258 m, 1153 w, 1028 w, 957 s, 885 m, 802 s, 751 s, 619 m, 569 m, 519 w, 431 s cm^{-1}; elemental analysis calcd (%) for $C_{52}H_{117}O_{19}N_3SnW_5$: C 30.58, H 5.36, N 1.94; found: C 30.29, H 5.37, N 2.06.

(TBA)$_3$ [(4-*t*BuC$_6$H$_4$O)SnW$_5$O$_{18}$], **(TBA)$_3$7** – A solution of 4-*tert*-butylphenol (0.025 g, 0.17 mmol) in acetonitrile (5 mL) was added to a solution of (TBA)$_3$**1** (0.31 g, 0.15 mmol) in acetonitrile (10 mL) and the mixture was heated at 90 °C for 64 h. After removal of volatiles under reduced pressure, the yellow residue was washed with dry THF (2 x 20 mL), dry toluene (2 x 20 mL) and dry diethyl ether (2 x 20 mL) to remove unreacted 4-*tert*-butylphenol. The pale yellow crude product was dried *in vacuo* and recrystallised from acetonitrile and diethyl ether to give yellow crystals. Yield 0.27 g, 81 %. ^{1}H NMR (300 MHz, [D$_3$]MeCN, Me$_4$Si): δ = 1.29 (s, 9H, C(CH_3)$_3$), 6.88 (m, 2H, C$_6H_4$) and 7.20 (m, 2H, C$_6H_4$); C{^{1}H} NMR (100.53 MHz, [D$_3$]MeCN, Me$_4$Si): δ = 158.3 (^2J(^{13}C,^{119,117}Sn) = 38.3 Hz, *ipso*-C$_6$H$_4$), 141.3 (*p*-C$_6$H$_4$), 125.7 (*m*-C$_6$H$_4$) and 119.4 (^3J(^{13}C,^{119,117}Sn) = 31.6 Hz, *o*-C$_6$H$_4$), 34.8 (*C*(CH$_3$)$_3$) and 31.94 (C(*C*H$_3$)$_3$); IR (Nujol): ν = 2727 m, 1603 m, 1509 s, 1377 s, 1256 m, 1183 m, 1152 m, 1108 m, 1068 w, 1026 w, 956 s, 884 m, 803 s, 754 s, 696 m, 622 m, 570 s cm^{-1}; elemental analysis calcd (%) for $C_{58}H_{121}N_3O_{19}SnW_5$: C 31.62, H 5.53, N 1.9; found: C 32.02, H 5.36, N 1.99.

(TBA)$_3$[(4-HOC$_6$H$_4$O)SnW$_5$O$_{18}$], **(TBA)$_3$8** – (TBA)$_3$**1** (0.60 g, 0.29 mmol) in dry acetonitrile (15 mL) was transferred to hydroquinone (0.067 g, 0.61 mmol) and the mixture was heated at 90 °C for 91 h. After removal of volatiles *in vacuo*, the sticky, pale red solid was washed with dry THF (4 x 20 mL)and dry diethyl ether(2 x 20 mL) to remove unreacted hydroquinone. The solid was dried *in vacuo* and recrystallised from acetonitrile and diethyl ether to give pale yellow crystals. Yield 0.47 g, 75%. ^{1}H NMR (300 MHz, [D$_3$]MeCN, Me$_4$Si): δ = 6.62 (m, 2H, C$_6H_4$), 6.68 (m, 2H, C$_6H_4$), 6.46 (br s, 1H, OH); C{^{1}H} NMR (100.53 MHz, [D$_3$]MeCN, Me$_4$Si): δ = 153.7 (*ipso*-C$_6$H$_4$), 149.7 (*p*-C$_6$H$_4$), 120.3 (*o*-C$_6$H$_4$) and 115.3 (*m*-C$_6$H$_4$); IR (Nujol): ν = 3294 br, 2726 m, 1377 s, 1307 w, 1238 w, 1153 m, 1027 w, 955 s, 885 w, 805 s, 754 s, 624 m, 570 w, 432 s cm^{-1}; elemental analysis calcd (%) for $C_{54}H_{113}O_{20}N_3SnW_5$: C 29.99, H 5.26, N 1.94; found: C 30.32, H 5.39, N 2.01.

(TBA)$_3$[(3-HOC$_6$H$_4$O)SnW$_5$O$_{18}$], **(TBA)$_3$9** – A solution of (TBA)$_3$**1** (0.77 g, 0.37 mmol) in acetonitrile (15 mL) was transferred to resorcinol (0.045 g, 0.41 mmol) and the reaction mixture was heated at 90 °C for 65 h. After removal of volatiles *in vacuo*, the sticky yellow residue was washed with dry THF (4 x 20 mL) and dry diethyl ether (2 x 20 mL) to remove unreacted resorcinol. The pale yellow solid was dried *in vacuo* and recrystallised from acetonitrile and diethyl ether to give yellow crystals. Yield 0.62 g, 78 %. ^{1}H NMR (300 MHz, [D$_3$]MeCN, Me$_4$Si): δ = 6.27 (m, 1H, C$_6H_4$), 6.46 (m, 1H, C$_6H_4$), 6.49 (m, 1H, C$_6H_4$), 6.86 (br s, 1H, OH) and 7.00 (m, 1H, C$_6H_4$); C{^{1}H} NMR (100.53 MHz, [D$_3$]MeCN, Me$_4$Si): δ = 106.1, 107.1, 111.9, 129.2, 157.8 and 162.0 (C$_6$H$_4$); IR (Nujol): ν = 3255 br, 2728 m, 1661 w, 1580 m, 1377 s, 1295 w, 1253 w, 1142 s, 1107 w, 1057 w, 1026 w, 953 s, 885 w, 799 s, 748 s, 619 m, 569 m, 427 m cm^{-1}; elemental analysis calcd (%) for $C_{54}H_{113}N_3O_{20}SnW_5$: C 29.99, H 5.26, N 1.94: found: C 29.60, H 5.3, N 2.04.

(TBA)$_3$[(2-CHOC$_6$H$_4$O)SnW$_5$O$_{18}$], **(TBA)$_3$10** – A solution of salicylaldehyde (0.58 ml, 0.54 mmol) in acetonitrile (5 mL) was added drop-wise to the solution of (TBA)$_3$**1** (0.97 g, 0.47 mmol) in acetonitrile (15 mL) with stirring. The reaction mixture was then heated at 90 °C for 48 h. After removal of volatiles under reduced pressure, the sticky, yellow solid was washed with dry THF (4 x 20 mL) and dry diethyl ether (2 x 20 mL) to remove unreacted salicyaldehyde. The pale yellow solid was dried *in vacuo* and recrystallised from acetonitrile and diethyl ether to give yellow crystals. Yield 0.63 g, 62 %. ^{1}H NMR (300 MHz, [D$_3$]MeCN, Me$_4$Si): δ = 6.90 (m, 1H, C$_6H_4$), 7.24 (m, 1H, C$_6H_4$), 7.48 (m, 1H, C$_6H_4$), 7.64 (m, 1H, C$_6H_4$) and 10.52 (s, 1H, CHO); C{^{1}H} NMR (100.53 MHz, [D$_3$]MeCN, Me$_4$Si): δ = 119.3, 122.9, 126.7, 127.1, 135.6, 164.9, (C$_6$H$_4$) and 190.8 (CHO); IR (Nujol): ν = 2728 m, 1679 m, 1597 m, 1378 s, 1315 m, 1247 m, 1308 w, 1240 m, 1153 m, 1027 m, 958 s, 884 m, 802 s, 751 s, 617 m, 573 m, 527 m, 432 s cm^{-1}; elemental analysis calcd (%) for $C_{55}H_{113}O_{20}N_3SnW_5$: C 30.38, H 5.24, N 1.93; found: C 29.50, H 5.61, N 2.1.

Acknowledgements

R.J.E. and M.P-B. acknowledge COST Action CM1203 (Polyoxometalate Chemistry for Molecular Nanoscience, PoCheMoN) for support. B.K. thanks the University of St. Andrews for studentship funding, and A.R.-F. thanks the Spanish Ministry of Science (CTQ2014-52774-P) and the Generalitat de Catalunya (2009SGR462 and XRQTC) for support.

Keywords: polyoxometalate synthesis • tin alkoxide • multinuclear NMR • bonding • DFT calculations

[1] A. Proust, B. Matt, R. Villanneau, G. Guillemot, P. Gouzerh, G. Izzet, *Chem. Soc. Rev.* **2012**, *41*, 7605-7622.

[2] a) W. Clegg, M. R. J. Elsegood, R. J. Errington, J. Havelock, *Dalton Trans.* **1996**, 681-690; b) B. Kandasamy, C. Wills, W. McFarlane, William Clegg, R. W. Harrington, A. Rodríguez-Fortea, J. M. Poblet, P. G. Bruce, R. J. Errington, *Chem. Eur. J.* **2012**, *18*, 59-62.

[3] R. J. Errington, L. Coyle, P. S. Middleton, C. J. Murphy, W. Clegg, R. W. Harrington, *J. Clust. Sci*, **2010**, *21*, 503-514.

[4] R. J. Errington, G. Harle, W. Clegg, R. W. Harrington, *Eur. J. Inorg. Chem.* **2009**, 5240-5246

[5] a) R. J. Errington, S. S. Petkar, P. S. Middleton, W. McFarlane, W. Clegg, R. W. Harrington, *Dalton Trans.* **2007**, 5211-5222; b) R. J. Errington, S. S. Petkar, P. S. Middleton, W. McFarlane, W. Clegg, R. A. Coxall, R. W. Harrington, *J. Am. Chem. Soc.* **2007**, *129*, 12181-12196; c) L. Coyle, P. S. Middleton, C. J. Murphy, W. Clegg, R. W. Harrington, R. J. Errington, *Dalton Trans.* **2012**, *41*, 971-981.

[6] R. J. Errington, S. S. Petkar, B. R. Horrocks, A. Houlton, L. H. Lie, S. N. Patole, *Angew. Chem., Int. Ed.* **2005**, *44*, 1254.

[7] a) D. C. Bradley, R. C. Mehrotra, D. P. Gaur, *Metal Alkoxides*, Academic Press, London, UK, **1978**; b) D. C. Bradley, R. C. Mehrotra, I. P. Rothwell, A. Singh, *Alkoxo and Aryloxo Derivatives of Metals*, Academic Press, London, UK, **2001**.

[8] G. D. Smith, P. E. Fanwick, I. P. Rothwell, *Inorg. Chem.* **1990**, *29*, 322-3226.

[9] M. Pascual-Borràs, X. López, A. Rodríguez-Fortea, R. J. Errington, J. M. Poblet, *Chem. Sci.* **2014**, *5*, 2031-2042.

[10] a) A. Bagno, M. Bonchio, *Angew. Chem. Int. Ed.* **2005**, *44*, 2023-2025; b) A. Bagno, M. Bonchio, J. Autschbach, *Chem. Eur. J.* **2006**, *12*, 8460-8471; c) J. Gracia, J. M. Poblet, J. Autschbach, L. P. Kazansky, *Eur. J. Inorg. Chem.* **2006**, 1139–1148; d) N. Vankova, T. Heine, U. Kortz, *Eur. J. Inorg. Chem.* **2009**, 5102–5108; e) D. Ravelli, D. Dondi, M. Fagnoni, A. Albini, A. Bagno, *J. Comput. Chem,* **2011**, *32*, 2983-2987; f) L. Vilà-Nadal, J. P. Sarasa, A. Rodríguez-Fortea, J. Igual, L. P. Kazansky, J. M. Poblet, *Chem. Asian J.* **2010**, *5*, 97-104.

[11] R. J. Errington, *Advanced Practical Inorganic and Metalorganic Chemistry*, Blackie Academic & Professional, London, **1997**.

[12] Oxford Diffraction CrysAlisPro software, 2009–2012.

[13] G. M. Sheldrick, *Acta Crystallogr. Sect. C* **2015**, *71*, 3–8.

[14] ADF2016. SCM, Theoretical Chemistry, Vrije Universiteit, Amsterdam, The Netherlands, http://www.scm.com. a) E. J. Baerends, D. E. Ellis, P. Ros, *Chem. Phys.* **1973**, *2*, 41-51; b) L. Versluis, T. Ziegler, *J. Chem. Phys.* **1988,** *88*, 322-328; c) G. Te Velde, E. J. Baerends, *J. Comput. Phys.* **1992**, *99*, 84-98; d) C. Fonseca Guerra, J. G. Snijders, G. Te Velde, E. J. Baerends, *Theor. Chem. Acc.* **1998,** *99*, 391-403.

Entry for the Table of Contents (Please choose one layout)

Layout 1:

FULL PAPER

Sn *versus* Ti: the effects of metal substitution on the bonding within a homologous series of $[(RO)MW_5O_{18}]^{3-}$ polyoxometalates have been revealed by combined structural, spectroscopic and theoretical studies of Ti and Sn derivatives, highlighting the influence of M–OR π-bonding on the distributed electronic effects within the oxide framework.

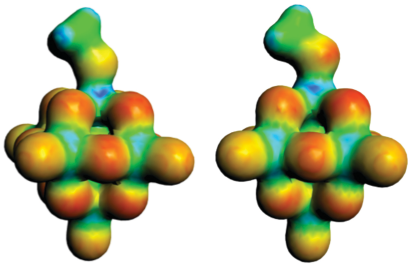

$[(MeO)TiW_5O_{18}]^{3-}$ $[(MeO)SnW_5O_{18}]^{3-}$

*Balamurugan Kandasamy, Peter G. Bruce, William Clegg, Ross W. Harrington, Antonio Rodríguez-Fortea, Magda Pascual-Borrás and R. John Errington**

Page No. – Page No.

Bonding insights from structural and spectroscopic comparisons of {SnW_5} and {TiW_5} alkoxido- and aryloxido-substituted Lindqvist polyoxometalates

Supporting Information

Contents

Spectroscopy

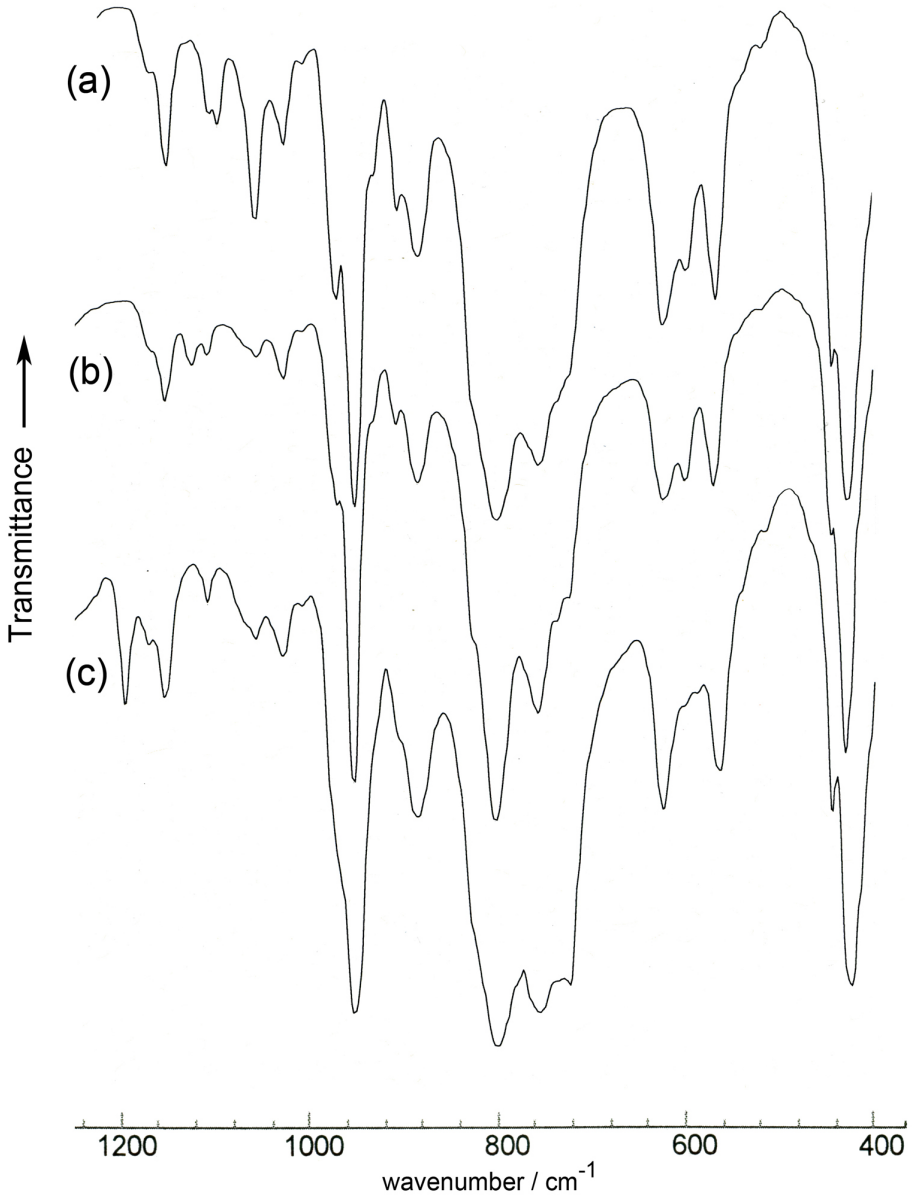

Figure S1. FTIR spectra of TBA salts of alkoxido anions (a) **2**, (b) **3** and (c) **4**..

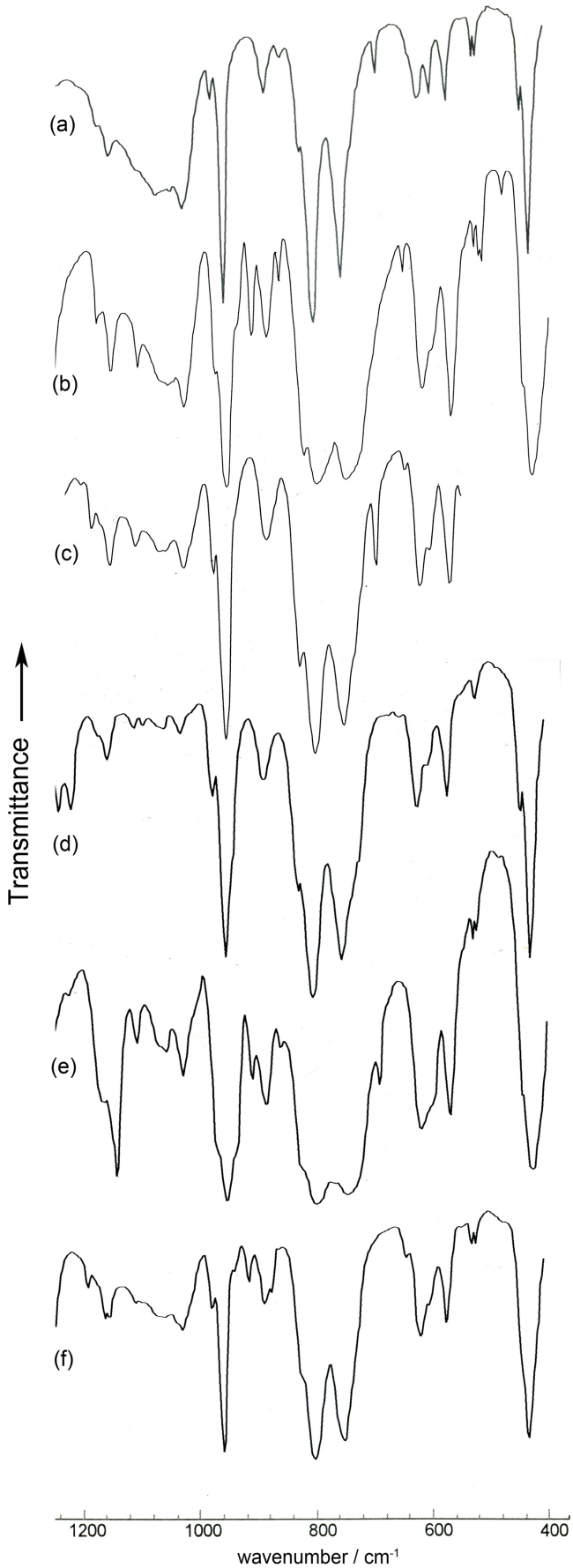

Figure S2. FTIR spectra of TBA salts of aryloxido anions (a) **5**, (b) **6**, (c) **7**, (d) **8**, (e) **9** and (f) **10**.

Table S1. NMR data for $\{XSnW_5\}$ polyoxometalates **1** - **10**

Anion[a]	^{119}Sn chemical shift/ppm	^{183}W chemical shift/ppm		^{17}O chemical shift/ppm			
	($^2J\{^{119}Sn\,^{183}W_{eq}\}$/Hz)	W_{eq}	W_{ax}	W=O	SnOW	WOW	μ_6-O
$[(MeO)SnW_5O_{18}]^{3-}$ **1**	–647 (38.4)	76.9	–128.1	720, 684	395	383, 363	17
$[(EtO)SnW_5O_{18}]^{3-}$ **2**	–651 (39.8)	74.7	–129.6	725, 684	395	382, 365	17
$[(^iPrO)SnW_5O_{18}]^{3-}$ **3**	–654 (39.9)	74.5	–128.3	726, 684	396	383, 367	18
$[(^tBuO)SnW_5O_{18}]^{3-}$ **4**	–663 (40.3)	71.8	–126.7	725, 683	396	382, 368	18
$[(C_6H_5O)SnW_5O_{18}]^{3-}$ **5**	–673 (45.6)	77.4	–124.1	723, 689	397	385, 361	16
$[(4\text{-}MeC_6H_4O)SnW_5O_{18}]^{3-}$ **6**	–674 (47.5)	78.9	–122.8	722, 688	396	385, 361	16
$[(4\text{-}^tBuC_6H_4O)SnW_5O_{18}]^{3-}$ **7**	–673 (45.6)	76.7	–121.6	723, 689	396	386, 362	17
$[(4\text{-}HOC_6H_4O)SnW_5O_{18}]^{3-}$ **8**	–674 (51.2)	76.4	–122.8	723, 689	398	386, 363	17
$[(3\text{-}HOC_6H_4O)SnW_5O_{18}]^{3-}$ **9**	–674 (45.6)	76.5	–123.1	723, 688	397	386, 362	16
$[\{2\text{-}(CHO)C_6H_4O\}SnW_5O_{18}]^{3-}$ **10**	–672 (48.9)	79.1	–120.6	725, 691	399	387, 365	15

[a] As $^nBu_4N^+$ salts.

Crystallography

Table S2. Crystallographic data for non-disordered structures.

	$(TBA)_3$**2**	$(TBA)_3$**3**	$(TBA)_3$**4**	$(TBA)_3$**5**	$(TBA)_3$**6**
Chemical formula	$3C_{16}H_{36}N^+$ $C_2H_5O_{19}SnW_5^{3-}$	$3C_{16}H_{36}N^+$ $C_3H_7O_{19}SnW_5^{3-}$	$3C_{16}H_{36}N^+$ $C_4H_9O_{19}SnW_5^{3-}$ $\cdot 0.5C_2H_3N$	$3C_{16}H_{36}N^+$ $C_6H_5O_{19}SnW_5^{3-}$	$3C_{16}H_{36}N^+$ $C_7H_7O_{19}SnW_5^{3-}$
Formula mass	2098.37	2112.40	2146.95	2146.41	2160.44
Crystal system	Monoclinic	Monoclinic	Monoclinic	Orthorhombic	Orthorhombic
a /Å	29.6464(14)	29.7267(5)	24.8325(6)	16.5832(3)	23.7204(3)
b /Å	18.5757(5)	37.2181(9)	33.8943(8)	17.7461(3)	17.1487(3)
c /Å	27.228(2)	27.2009(5)	16.9063(4)	23.6843(3)	17.1872(2)
β /°	112.783(8)	112.835(2)	91.325(2)	90.0	90.0
Unit cell volume /Å^3	13824.6(13)	27735.7(10)	14225.9(6)	6969.99(19)	6991.31(17)
Space group	*C*2/*c*	$P2_1/c$	$P2_1/c$	$P2_12_12_1$	*Pnma*
Z	8	16	8	4	4
μ /mm^{-1}	8.705	8.679	8.462	8.636	8.610
Crystal size /mm	0.40 × 0.40 × 0.40	0.50 × 0.40 × 0.40	0.43 × 0.20 × 0.20	0.34 × 0.30 × 0.30	0.20 × 0.15 ×0.15
Transmission range	0.105–0.130	0.098–0.129	0.121–0.282	0.157–0.182	0.278–0.358
Reflections measured	47841	148389	79553	41217	40251
Unique reflections	13716	48896	25072	13481	7333
R_{int} (on F^2)	0.0571	0.0744	0.0730	0.0516	0.0458
No. of refined parameters	836	2845	1463	760	473
No. of restraints	1450	12028	3213	985	490
R [F, $F^2 > 2\sigma(F^2)$]	0.0511	0.0878	0.0569	0.0300	0.0323
R_w (F^2, all data)	0.0799	0.1415	0.1179	0.0472	0.0550
Goodness of fit on F^2	1.025	1.052	1.027	0.853	1.026
Difference map extremes /e Å^{-3}	1.78, −1.21	10.14, −4.12	3.36, −2.31	0.96, −1.16	1.48, −1.71

Table S2. Crystallographic data for non-disordered structures (continued)

	$(TBA)_3$**7**	$(TBA)_3$**8**	$(TBA)_3$**9**	$(TBA)_3$**10**
Chemical formula	$3C_{16}H_{36}N^+$ $C_{10}H_{13}O_{19}SnW_5^{3-}$	$3C_{16}H_{36}N^+$ $C_6H_5O_{20}SnW_5^{3-}$	$3C_{16}H_{36}N^+$ $C_6H_5O_{20}SnW_5^{3-}$	$3C_{16}H_{36}N^+$ $C_7H_5O_{20}SnW_5^{3-}$
Formula mass	2202.52	2162.41	2162.41	2174.42
Crystal system	Orthorhombic	Monoclinic	Monoclinic	Orthorhombic
a /Å	2496.50(5)	18.4269(6)	18.135(2)	23.4632(8)
b /Å	16.9285(3)	15.1562(5)	15.4851(9)	17.1341(7)
c /Å	17.7849(4)	25.0820(9)	25.016(5)	17.4416(5)
β /°	90.0	90.775(3)	91.18(2)	90.0
Unit cell volume /Å^3	7516.3(3)	7004.3(4)	7023.6(17)	7011.9(4)
Space group	*Pna*2$_1$	*C*2/*c*	*I*2/*a*	*Pnma*
Z	4	4	4	4
μ /mm^{-1}	8.011	8.595	8.572	8.587
Crystal size /mm	0.32 × 0.30 × 0.30	0.25 × 0.20 × 0.20	0.50 × 0.40 × 0.40	0.30 × 0.30 × 0.20
Transmission range	0.184–0.197	0.223–0.278	0.100–0.131	0.183–0.279
Reflections measured	54619	21103	24618	53911
Unique reflections	13810	6176	6102	7414
R_{int} (on F^2)	0.0347	0.0533	0.0605	0.1839
No. of refined parameters	776	484	484	479
No. of restraints	1024	568	556	631
R [F, $F^2 > 2\sigma(F^2)$]	0.0342	0.0712	0.0478	0.1127
R_w (F^2, all data)	0.0455	0.1202	0.0882	0.1318
Goodness of fit on F^2	1.025	1.050	1.036	1.153
Difference map extremes /e Å^{-3}	1.47, −1.43	2.49, −2.42	2.25, −1.51	3.28, −7.71

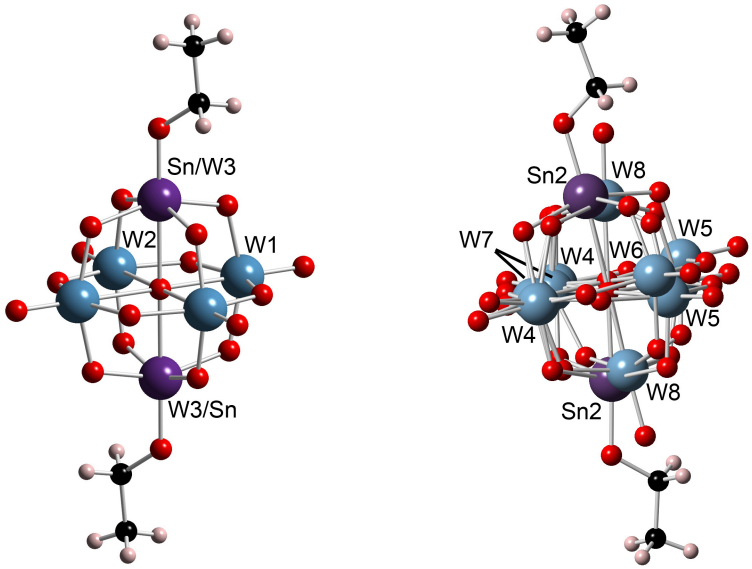

Figure S3. Structures of the disordered anions in the crystal strucure of $(TBA)_3$**2**.

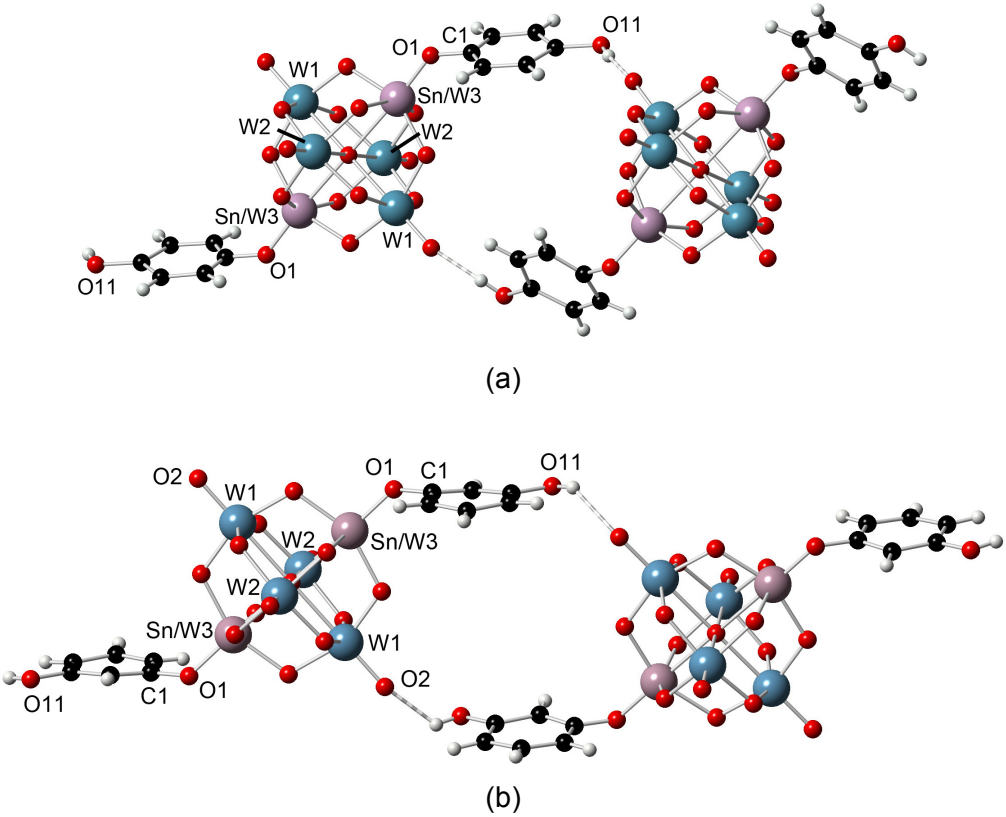

Figure S4. Structures of the disordered anions in the crystal strucures of (a) $(TBA)_3$**8** and (b) $(TBA)_3$**9**.

Table S3. Average bond lengths (Å) and selected angles (°) for non-disordered anions in $(TBA)_3[XSnW_5]$ polyoxometalate structures.[a]

	Anion									
	3(a)	**3(b)**	**3(c)**	**3(d)**	**4(a)**	**4(b)**	**5**	**6**	**7**	**10**
Sn–O	1.931(15)	1.947(14)	1.961(16)	1.949(16)	1.988(10)	1.977(11)	1.961(4)	1.954(5)	1.995(6)	1.980(2)
O–C	1.38(3)	1.36(3)	1.37(3)	1.39(3)	1.284(15)	1.259(17)	1.357(8)	1.371(10)	1.330(11)	1.38(5)
SnOC	126.4(16)	126.7(15)	121.7(15)	120.9(15)	134.2(9)	139.3(12)	128.4(4)	129.2(6)	127.4(6)	127(2)
$Sn–O_c$	2.031(15)	2.035(14)	2.046(15)	2.027(15)	2.048(10)	2.044(11)	2.025(4)	2.025(4)	2.034(8)	2.009(16)
$Sn–O_f$	2.261(13)	2.260(13)	2.256(14)	2.214(14)	2.272(8)	2.275(8)	2.241(4)	2.237(4)	2.196(4)	2.25(2)
$O_fSnO(C)$	174.7(6)	175.2(6)	177.6(6)	177.8(6)	176.6(5)	172.6(5)	177.7(2)	177.7(2)	175.0(2)	179.5(10)
SnO_fW_{ax}	179.3(6)	179.5(6)	179.6(8)	178.6(7)	179.6(4)	180.0(5)	179.50(19)	179.6(2)	179.7(5)	178.7(10)
$W_{eq}–O_a$	1.722(14)	1.712(14)	1.723(15)	1.717(15)	1.707(8)	1.711(12)	1.702(5)	1.707(4)	1.712(8)	1.712(17)
$W_{ax}–O_b$	1.729(13)	1.728(13)	1.741(15)	1.739(15)	1.711(9)	1.735(9)	1.731(4)	1.757(6)	1.711(5)	1.80(2)
$W_{eq}–O_c$	1.854(14)	1.863(13)	1.870(16)	1.876(16)	1.860(10)	1.866(10)	1.866(4)	1.869(4)	1.855(8)	1.897(16)
$W_{eq}–O_d$	1.976(14)	1.969(13)	1.958(15)	1.920(16)	1.959(8)	1.948(9)	1.949(5)	1.947(4)	1.952(8)	1.970(16)
$W_{ax}–O_d$	1.902(14)	1.906(13)	1.902(15)	1.920(14)	1.907(8)	1.917(10)	1.921(4)	1.914(4)	1.902(8)	1.925(16)
$W_{eq}–O_e$	1.934(14)	1.939(14)	1.925(15)	1.934(15)	1.930(9)	1.932(11)	1.935(5)	1.930(4)	1.935(9)	1.937(17)
$W_{eq}–O_f$	2.337(13)	2.338(13)	2.336(14)	2.336(14)	2.337(8)	2.330(8)	2.342(5)	2.341(3)	2.338(9)	2.345(14)
$W_{ax}–O_f$	2.356(13)	2.353(13)	2.344(14)	2.381(14)	2.361(8)	2.365(8)	2.352(4)	2.351(4)	2.397(4)	2.34(2)

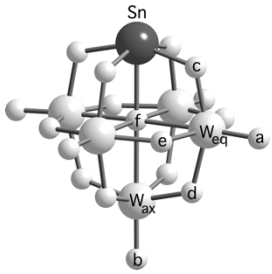

[a] Average values shown for O_a, O_c, O_d and O_e sites.

Computational analysis

Calculations of ^{183}W NMR chemical shifts were performed for two models (both with C_s symmetry) so as to simulate the rotation of the -CH_3 group around the O−Sn bond. In the first model, the C−O−Sn−O dihedral is 0° (*eclipsed*), whereas in the second the same dihedral angle is 45° (*staggered*). The results for the shieldings and the chemical shifts are shown in Table S5 and results for calculations of spin-spin Sn-W coupling constants, *K*(Sn-W) and *J*(Sn-W) are shown in Table S6.

Table S4. Computed ^{183}W shieldings and chemical shifts for the two models of $[(MeO)MW_5O_{18}]^{3-}$, along with the experimental values for the shifts (ppm). The computed shielding for the WO_4^{2-} reference is 2556.64 ppm.

	Eclipsed	Staggered
$\sigma(W_{ax})$	2641.18	2647.11
$\sigma(W_{eq,1})$	2451.60	2455.20
$\sigma(W_{eq,2})$	2443.38	2449.58
$\sigma(W_{eq,3})$	2454.54	-
$\sigma(W_{eq})_{av}$	2449.84	2452.39
$\delta(W_{ax})$	−84.54	−90.47
$\delta_{exp}(W_{ax})$	−120	−120
$d(W_{eq})_{av}$	106.80	104.15
$\delta_{exp}(W_{eq})$	70	70
$\Delta\delta$ (W_{eq-ax})	191	195
$\Delta\delta_{exp}(W_{eq-ax})$	190	190

Table S5. Computed spin-spin Sn-W coupling constants, *K*(Sn-W) and *J*(Sn-W), for the two models of $[(MeO)MW_5O_{18}]^{3-}$, along with the experimental values for *J*(Sn-W).

	Eclipsed		Staggered	
	$K^{a)}$	$J^{b)}$	$K^{a)}$	$J^{b)}$
Sn-W_{ax}	50.29	−9.47	47.88	−9.02
Sn-$W_{eq,1}$	186.89	−35.21	191.78	−36.13
Sn-$W_{eq,2}$	201.56	−37.97	220.80	−41.59
Sn-$W_{eq,3}$	257.53	−48.51	-	-
Sn-$W_{eq,av}$	215.33	−40.56	206.29	−38.86
$(Sn-W_{ax})_{exp}$		12		12
$(Sn-W_{eq})_{exp}$		38		38

a) *K* in 10^{19} kg $m^{-2}s^{-2}A^{-2}$. b) *J* in Hz. It is not possible to assign the sign of *J* from the experiments.

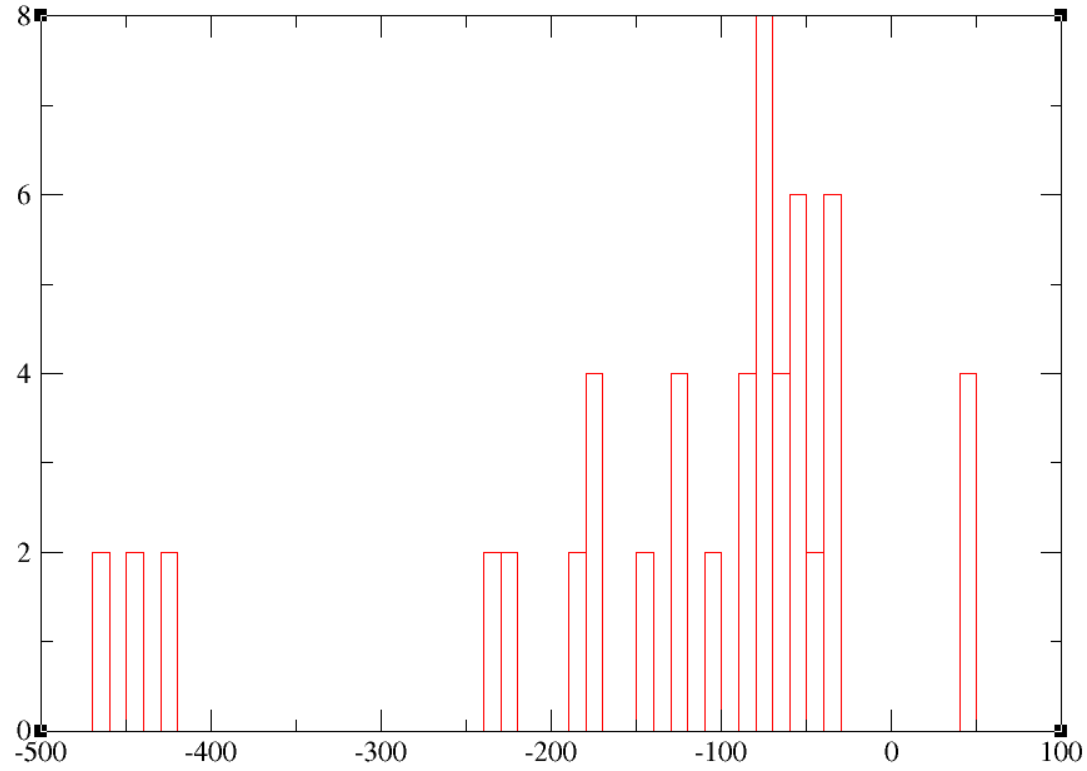

M = Sn

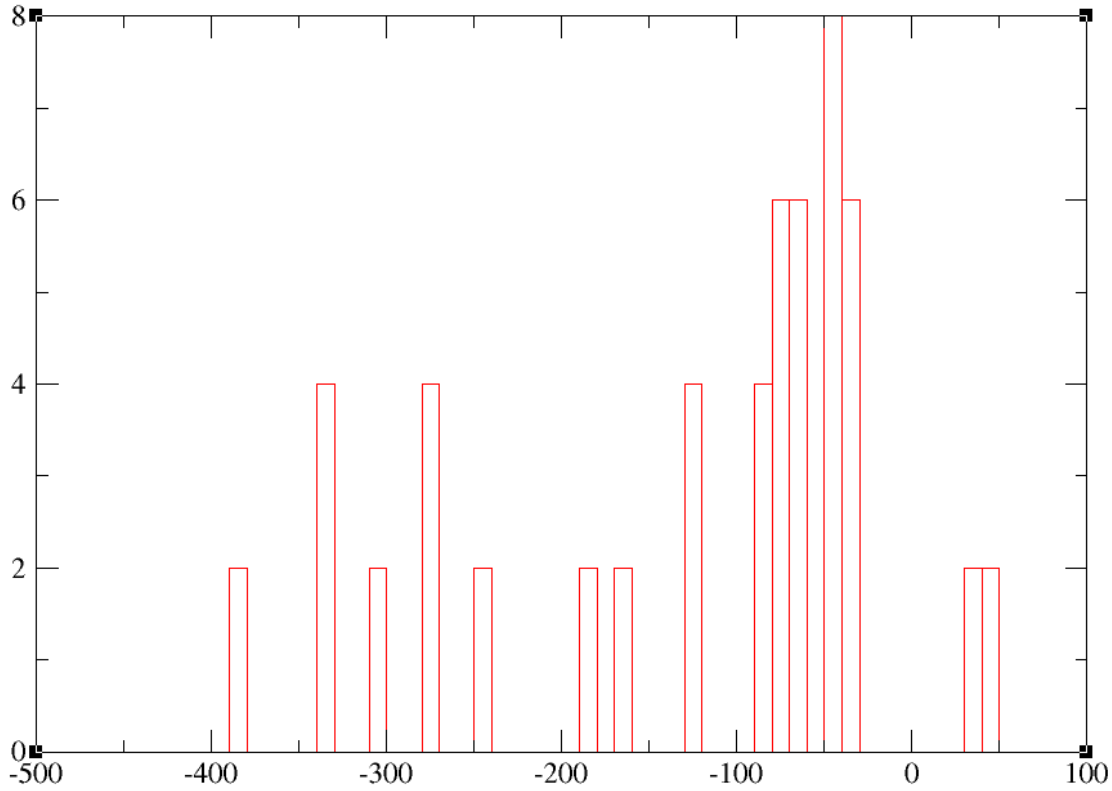

M = Ti

Fig. S5 Histograms of the occupied – virtual molecular orbital contributions (> 4%) to ^{183}W NMR paramagnetic shielding σ_p for $[(MeO)MW_5O_{18}]^{3-}$ anions. The large number of contributions to the total paramagnetic shielding σ_p with no clear dominant terms prevent a simple chemical explanation for these results.